Receptor interacting protein kinase 2-mediated mitophagy regulates inflammasome activation during virus infection

Christopher Lupfer[1], Paul G. Thomas[1], Paras K. Anand[1], Peter Vogel[3], Sandra Milasta[1], Jennifer Martinez[1], Gonghua Huang[1], Maggie Green[1], Mondira Kundu[2], Hongbo Chi[1], Ramnik J. Xavier[4,5,6], Douglas R. Green[1], Mohamed Lamkanfi[7,8], Charles A. Dinarello[9], Peter C. Doherty[1,10], Thirumala-Devi Kanneganti[1]

[1]Department of Immunology, [2]Department of Pathology and [3]Veterinary Pathology Core, St. Jude Children's Research Hospital, Memphis, TN 38105, United States.

[4]Gastrointestinal Unit and Center for the Study of Inflammatory Bowel Disease, and [5]Center for Computational and Integrative Biology, Massachusetts General Hospital, Harvard Medical School, Boston, Massachusetts 02114, United States.

[6]The Broad Institute of MIT and Harvard, 7 Cambridge Center, Cambridge, Massachusetts 02142, United States.

[7]Department of Biochemistry, Ghent University, and [8] Department of Medical Protein Research, VIB, B-9000 Ghent, Belgium.

[9]Department of Medicine, University of Colorado Denver, Aurora, CO 80045, United States.

[10]Department of Microbiology and Immunology, University of Melbourne, Vic 3010, Australia.

Correspondence should be addressed to:

Thirumala-Devi Kanneganti

Department of Immunology, MS #351

St Jude Children's Research Hospital

262 Danny Thomas Place

Memphis TN 38105-2794, USA

Tel: (901) 595-3634; FAX: (901) 595-5766

E-mail: Thirumala-Devi.Kanneganti@stjude.org

a

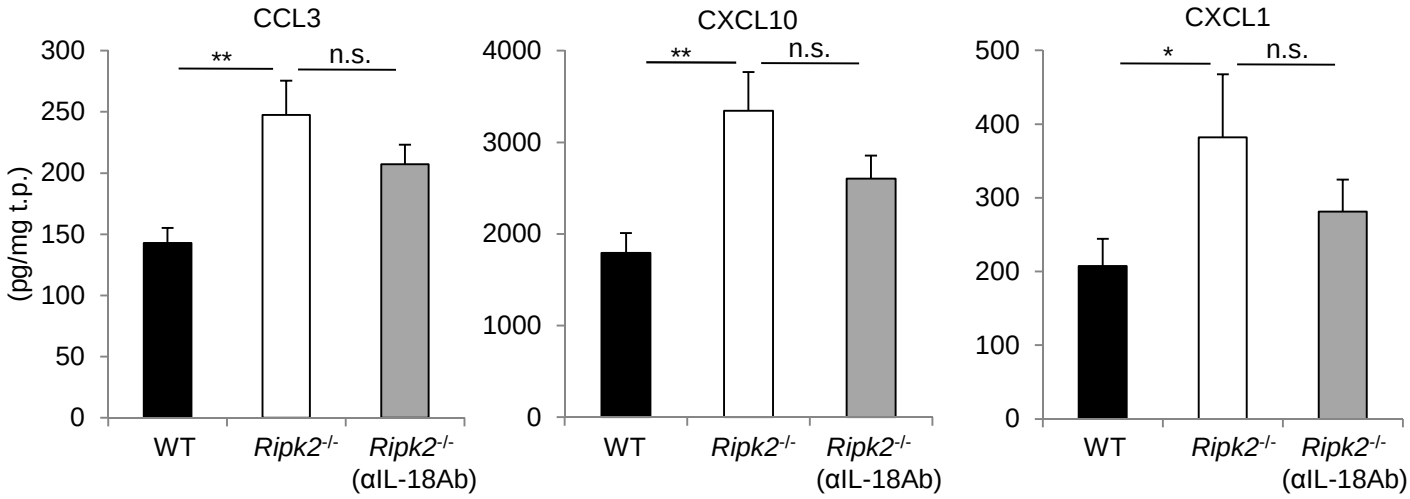

b

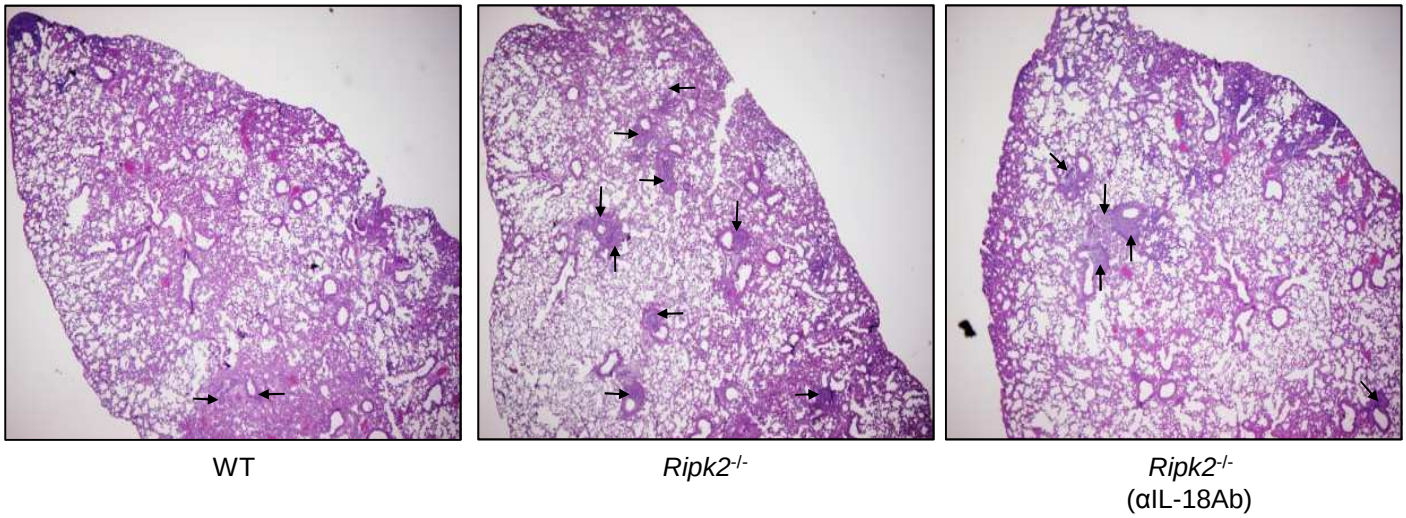

Supplemental Figure 1: Mitigation of pathology by IL-18 neutralization in *Ripk2*$^{-/-}$ mice. (**a**) CCL3, CXCL10 and CXCL1 levels following IL-18 neutralization (αIL-18Ab) in PR8-infected mice. Data were normalized to total protein from homogenates (pg/mg total protein (t.p.)). (**b**) H&E stained lung sections from d2 after PR8 infection for WT, *Ripk2*$^{-/-}$, and *Ripk2*$^{-/-}$ mice treated with neutralizing antiserum to IL-18 (arrows indicate occluded airways). Data are cumulative from 2 independent experiments (mean +/-SEM, n=10-12 mice, *p<0.05, **p<0.01).

Supplemental Fig. 1

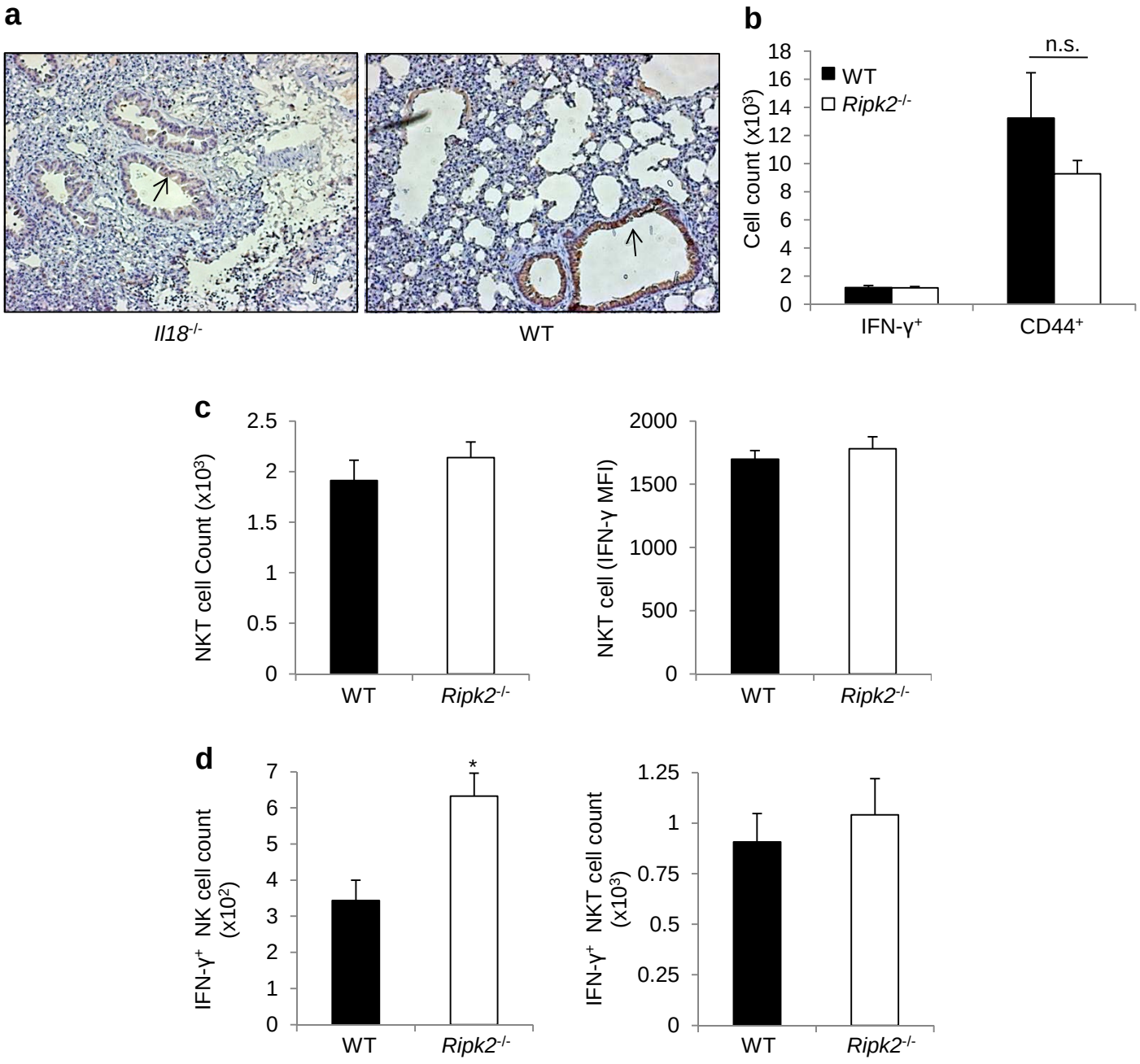

Supplemental Figure 2: NK, NKT and CD8⁺ T cell numbers are not affected by RIPK2 deficiency. (**a**) Control IL-18 IHC was performed on lungs from *IL18*$^{-/-}$ or WT mice and demonstrates staining only in WT mice (arrows indicate bronchial epithelium). (**b**) The total counts for lung CD8⁺ T cells expressing IFN-γ or CD44 in WT and *Ripk2*$^{-/-}$ mice on d7 after PR8 challenge. (**c**) The total counts on d2 after infection for lung NKT cells and the IFN-γ MFI of NKT cells for WT and *Ripk2*$^{-/-}$ mice. (**d**) IFN-γ⁺ NK and NKT cell numbers on d2 after infection in WT and *Ripk2*$^{-/-}$ mice. Data are cumulative from 2-3 independent experiments (mean +/-SEM, n=10-20 mice, *p<0.05).

Supplemental Fig. 2

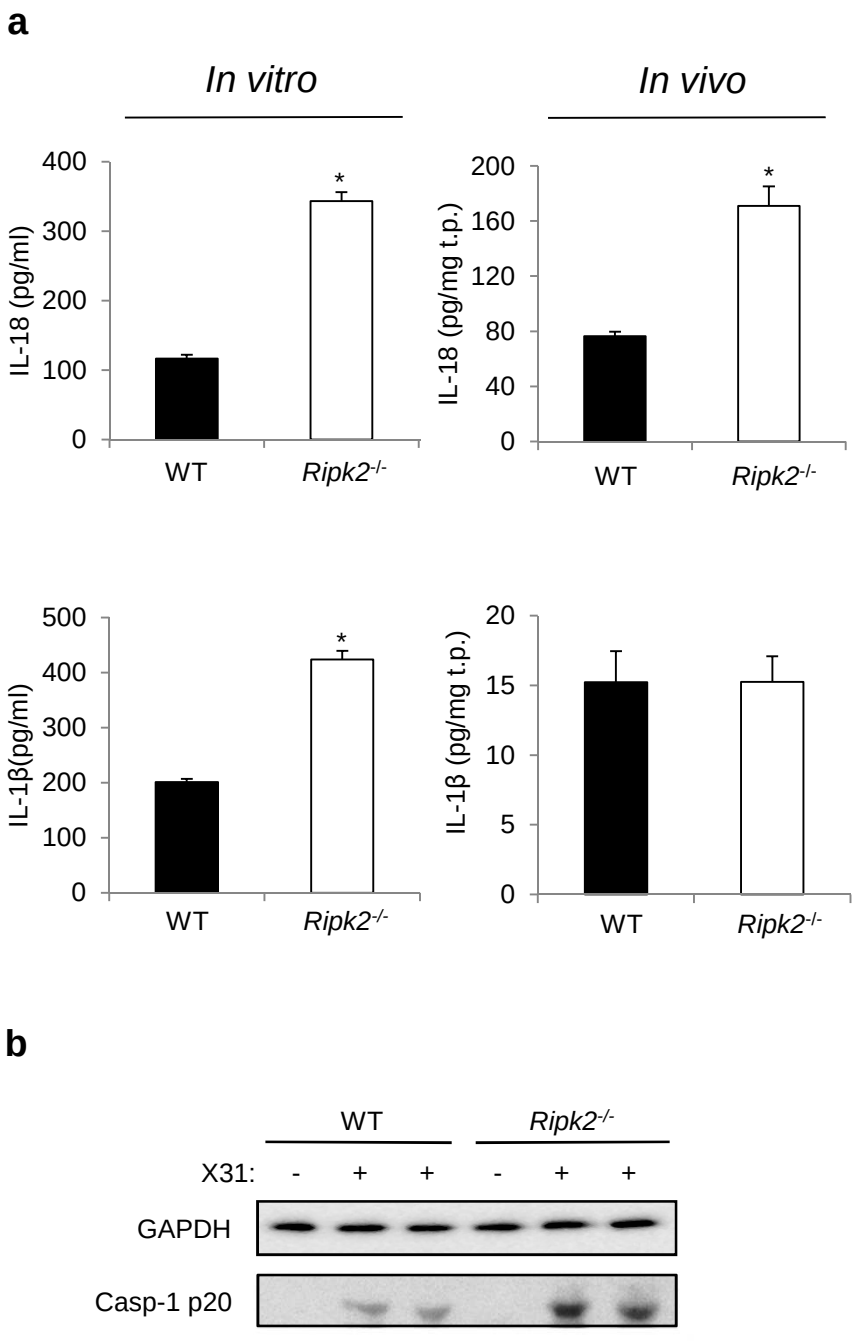

Supplemental Figure 3: IL-1β is regulated differentially *in vitro* and *in vivo*. (**a**) IL-1β and IL-18 levels in WT and *Ripk2*$^{-/-}$ BMDCs *in vitro* or *in vivo* on d2 following PR8 infection. (**b**) Casp-1 p20 levels in WT and *Ripk2*$^{-/-}$ BMDCs in response to the low pathogenicity X31 IAV. Data are representative of 2-3 independent experiments with n=2-3 per experiment for *in vitro* data and are cumulative from 3 experiments for *in vivo* data with n=10-12. (mean +/-SEM, *p<0.01)

Supplemental Fig. 3

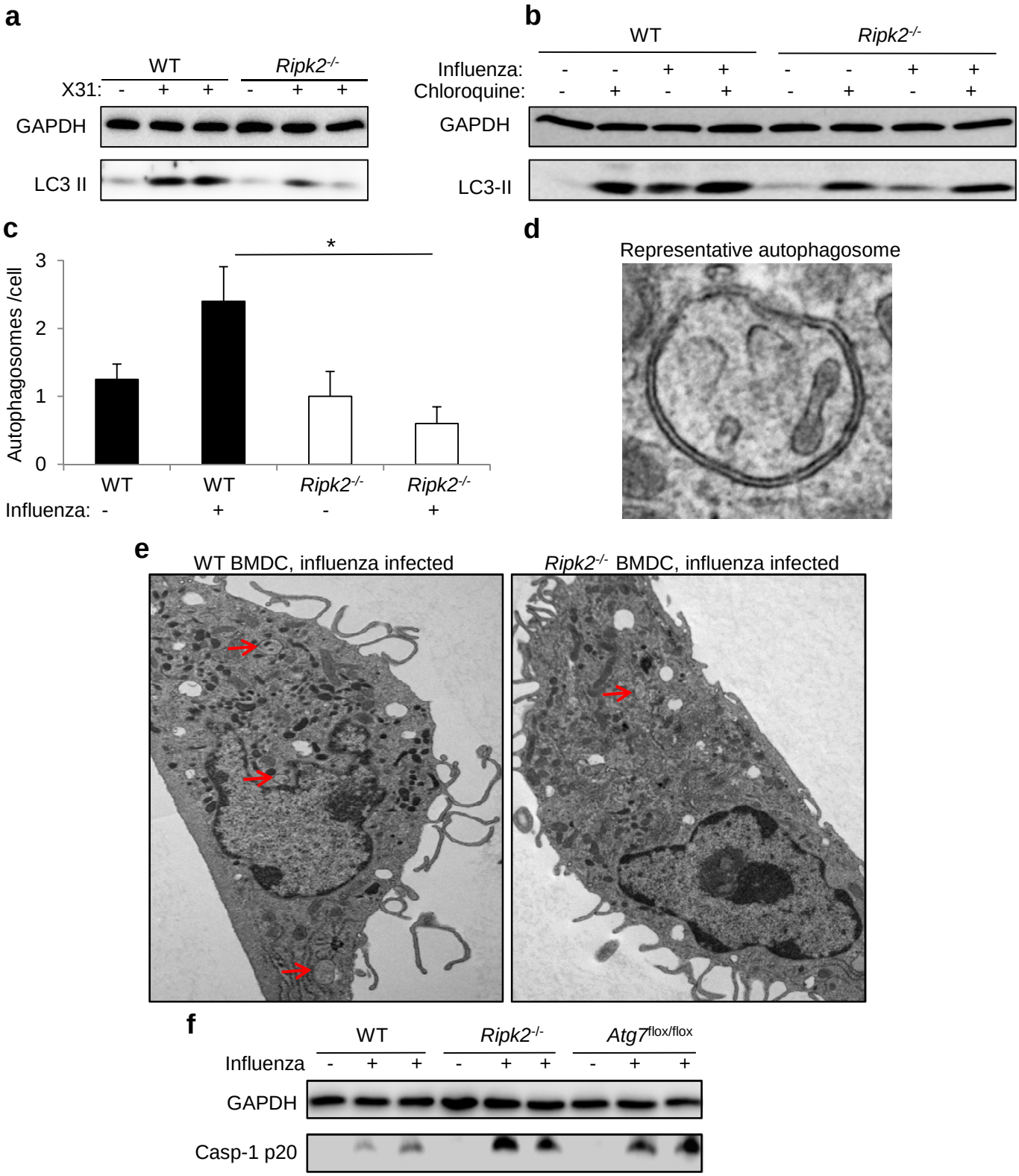

Supplemental Figure 4: Autophagic flux is normal in WT BMDCs following IAV infection. (**a**) Immunoblot of LC3-II conversion following X31 IAV infection of WT and *Ripk2*$^{-/-}$ BMDCs. (**b**) Immunoblots for LC3-II following PR8 infection and chloroquine treatment of WT and *Ripk2*$^{-/-}$ BMDCs. (**c-e**) Quantification of electron micrographs as well as electron micrographs showing autophagosomes in IAV infected WT or *Ripk2*$^{-/-}$ BMDCs after PR8 infection (red arrows indicate autophagosomes). (**f**) BMDMs with a conditional deletion for the autophagy gene *Atg7* were analyzed for casp-1 activation by immunoblot. (a-b, f) Data are representative of 3 independent experiments. (Mean +/- SEM, * $p<0.05$)

Supplemental Fig. 4

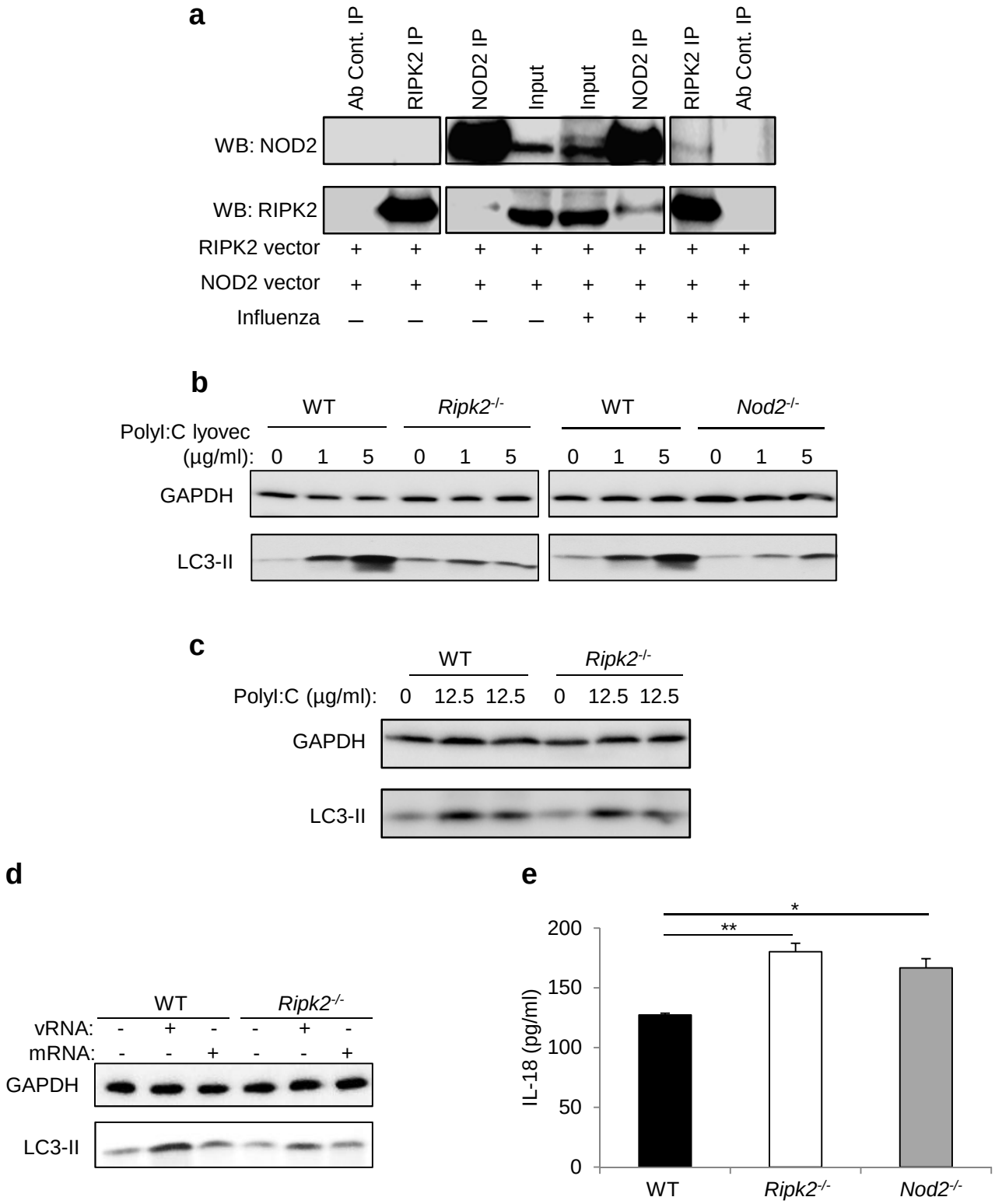

Supplemental Figure 5: Viral RNA genomes activate NOD2/RIPK2 mediated autophagy. (**a**) Immunoblots of coimmunoprecipitation of RIPK2 and NOD2. (**b**) Immunoblots of LC3-II conversion in WT, *Ripk2*$^{-/-}$ and *Nod2*$^{-/-}$ BMDCs following cytosolic delivery of poly I:C by lyovec transfection. (**c**) Immunoblots of LC3-II conversion in WT and *Ripk2*$^{-/-}$ BMDCs following extracellular treatment with Poly I:C. (**d**) LC3-II conversion following transfection of purified IAV genomes in WT and *Ripk2*$^{-/-}$ BMDCs. Cellular mRNA was transfected as a control. (**e**) IL-18 levels in WT, *Ripk2*$^{-/-}$ and *Nod2*$^{-/-}$ BMDCs following transfection of IAV genomes into BMDCs and ATP treatment. (a-e) Data are representative of 2-3 independent experiments with total n=3-6. (Mean +/- SEM, * $p<0.05$, ** $p<0.01$)

Supplemental Fig. 5

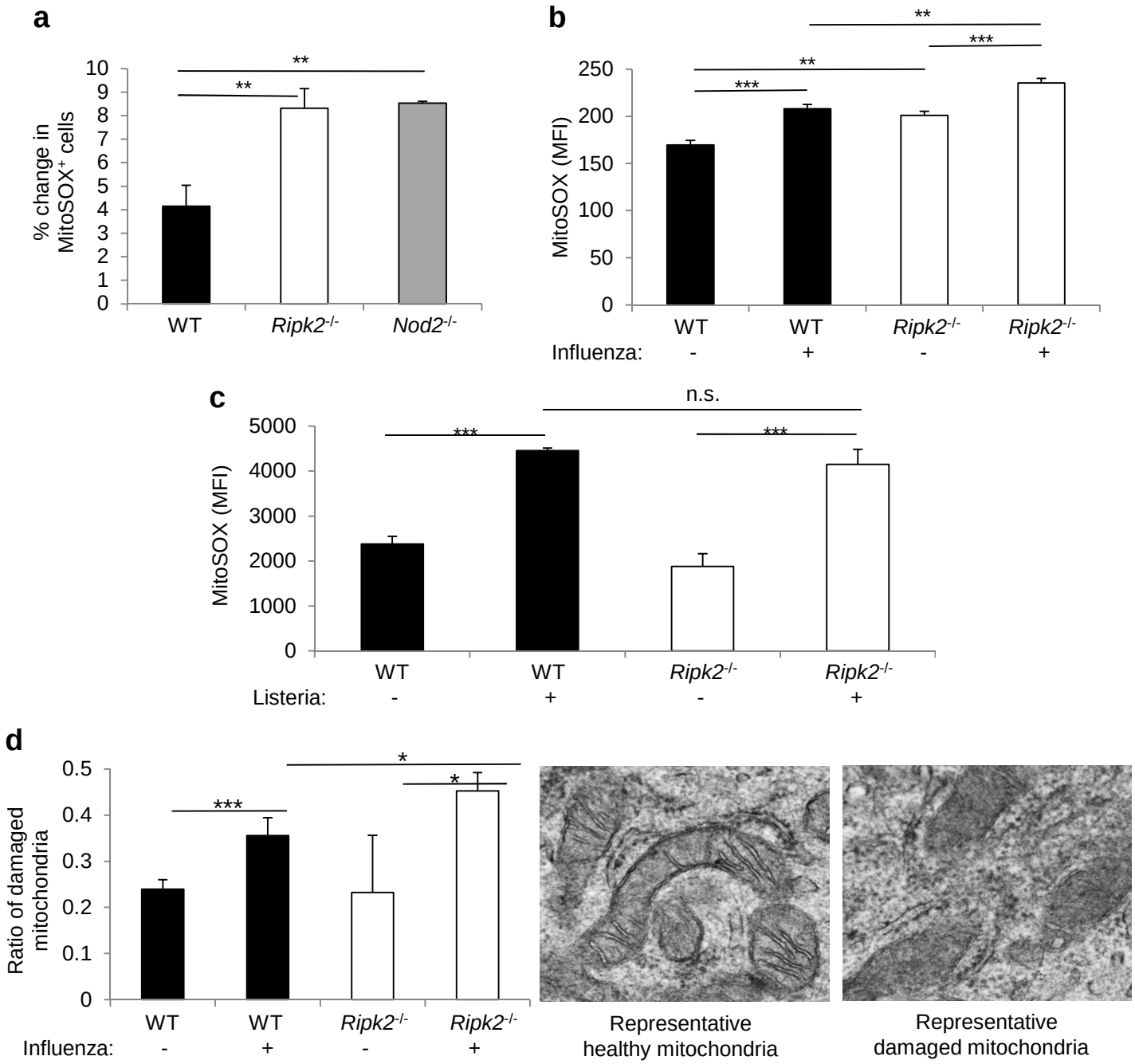

Supplemental Figure 6: *Ripk2*$^{-/-}$ BMDCs have increased mitochondrial damage during IAV infection but not Listeria infection. (**a**) The percent increase in MitoSOX positive cells following IAV infection in WT, *Ripk2*$^{-/-}$ and *Nod2*$^{-/-}$ BMDCs. (**b, c**) The geometric mean fluorescence intensity (MFI) of MitoSOX in WT and *Ripk2*$^{-/-}$ BMDCs during IAV or *Listeria* infection. (**d**) Quantification of damaged mitochondria was performed by transmission electron microscopy in uninfected or IAV infected BMDCs and expressed as the ratio of damaged to healthy mitochondria per cell. (a-c) Data are representative of 2-3 independent experiments with total n=4-6. (Mean +/- SEM, * $p<0.05$, ** $p<0.01$, *** $p<0.001$, n.s.=not significant)

Supplemental Fig. 6

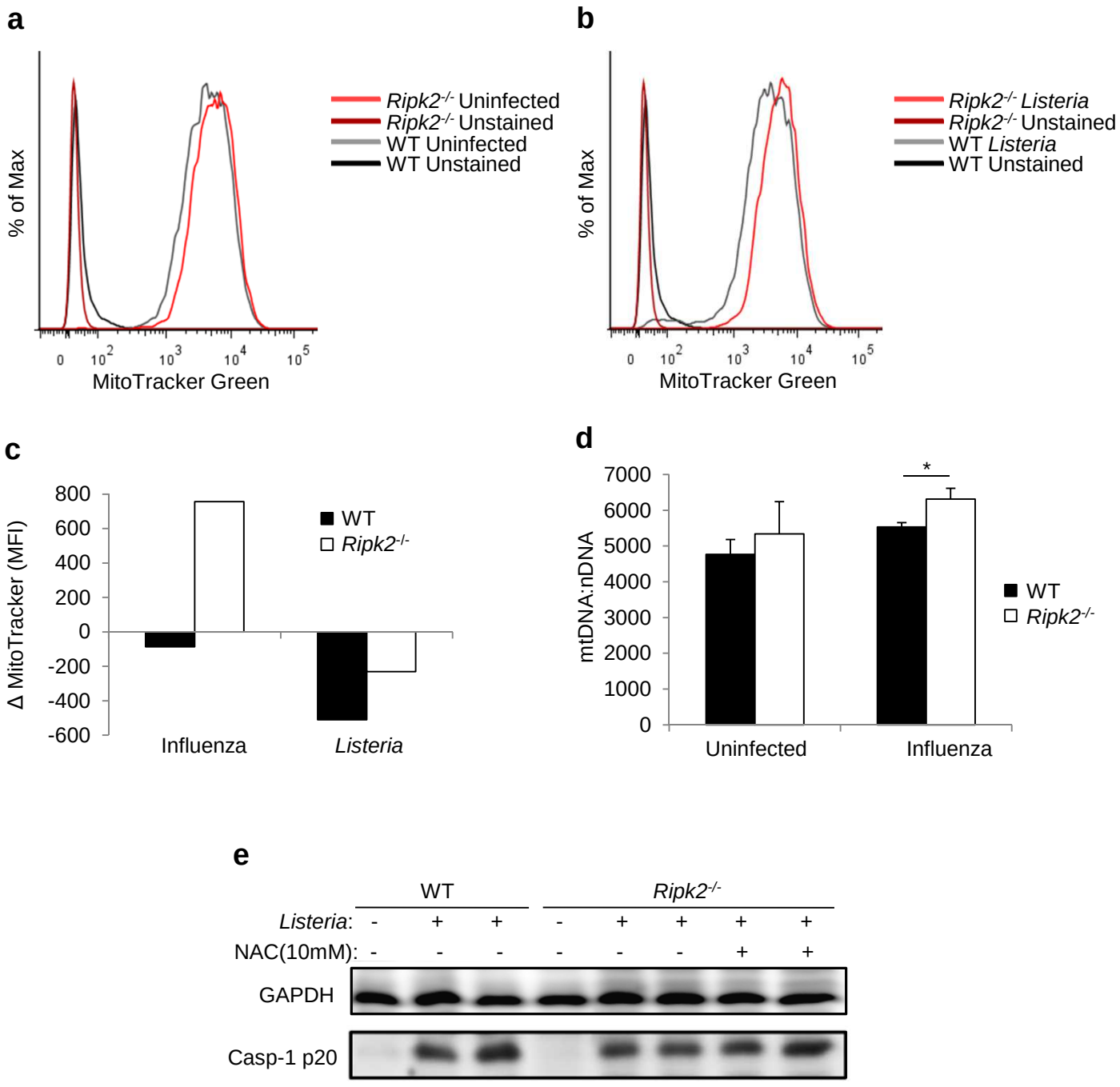

Supplemental Figure 7: *Ripk2*$^{-/-}$ BMDCs have increased mitochondrial mass following IAV infection. (**a-b**) MitoTracker Green staining of uninfected and Listeria infected BMDCs. (**c**) The change in MitoTracker Green MFI between uninfected and infected cells during PR8 or *Listeria* infection. (**d**) BMDCs were uninfected or infected with PR8 and the ratio of mitochondrial DNA (mtDNA) to nuclear DNA (nDNA) determined by qPCR. (**e**) Immunoblots of casp-1 p20 levels following treatment of WT and *Ripk2*$^{-/-}$ BMDCs with the ROS scavenger NAC during *Listeria* infection. Data are representative of 2-4 independent experiments with n=2-3 per experiment (mean +/- SEM, *p<0.05).

Supplemental Fig. 7

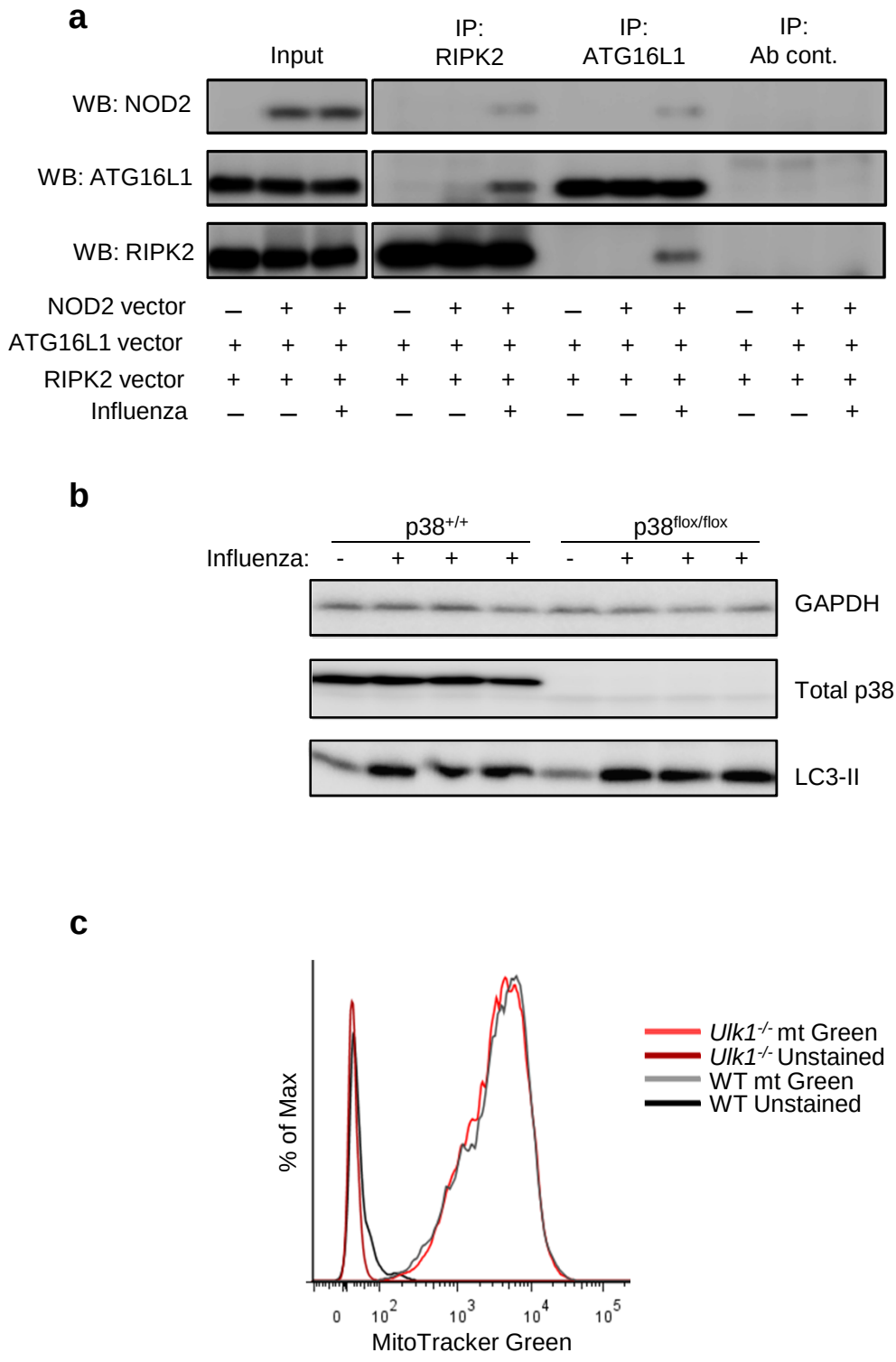

Supplemental Figure 8: RIPK2 regulates autophagy through Ulk1. (**a**) Coimmunoprecipitation of ATG16L1 with RIPK2 in the presence and absence of NOD2 and IAV infection. (**b**) The effects of p38 deletion on LC3-II conversion shown by immunoblot during PR8 infection. (**c**) Flow cytometry of MitoTracker Green in uninfected *Ulk1*$^{-/-}$ BMDCs. Data are representative of 2-3 independent experiments for a total n=3-6.

Supplemental Fig. 8